

Article

Not peer-reviewed version

Blackening Mechanism of Zn-Mg-Al Alloy Coated Steel Pre-pared by Water Vapor Treatment

[Sang-hee Kim](#) , You-jin Kang , Kyung-hwang Lee , [Jun Kang](#) , [Myeong-hoon Lee](#) , [Yong-sup Yun](#) *

Posted Date: 8 December 2023

doi: 10.20944/preprints202312.0634.v1

Keywords: ZnO; ZnO_{1-x}; Oxidation; Oxygen-deficient oxide; Optical bandgap energy



Preprints.org is a free multidiscipline platform providing preprint service that is dedicated to making early versions of research outputs permanently available and citable. Preprints posted at Preprints.org appear in Web of Science, Crossref, Google Scholar, Scilit, Europe PMC.

Copyright: This is an open access article distributed under the Creative Commons Attribution License which permits unrestricted use, distribution, and reproduction in any medium, provided the original work is properly cited.

Article

Blackening Mechanism of Zn-Mg-Al Alloy Coated Steel Prepared by Water Vapor Treatment

Sang-hee Kim ¹, Yu-jin Kang ², Kyung-hwang Lee ³, Jun Kang ⁴, Myeong-hoon Lee ⁴ and Yong-sup Yun ^{1,*}

¹ Department of Coast Guard Studies, Korea Maritime and Ocean University, Busan 49112, Republic of Korea

² KOMSA, Sejong 30100, Republic of Korea

³ Steel Solution R&D Center, POSCO, Incheon 21985, Republic of Korea

⁴ Department of Marine Engineering, Korea Maritime and Ocean University, Busan 49112, Republic of Korea

* Correspondence: ysyun@kmou.ac.kr

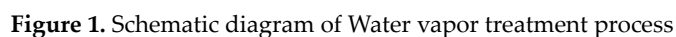
Abstract: In the context of high-temperature water vapor treatment, Zn-Mg-Al alloy-coated steel sheets exhibit the emergence of a black surface. This study aims to explore the factors and mechanisms contributing to surface blackening by inducing black surfaces on Zn-Mg-Al alloy-coated steel sheets, which were fabricated through molten coating subjected to water vapor treatment at 150 degrees Celsius. The surfaced composition was predominantly identified as ZnO, a zinc oxide film, validated through X-ray diffraction (XRD) and X-ray photoelectron spectroscopy (XPS). Morphological analysis of the surface and cross-section post-water vapor treatment revealed a disrupted lamellar structure with diffused features, resulting in the formation of an oxide film. Optical properties analysis demonstrated an increased absorbance and a decreased bandgap energy after water vapor treatment, indicative of an augmented blackening effect. Consequently, the high-temperature water vapor treatment led to the formation of oxides on the surface, with the highly reactive Mg and Al extracting oxygen from the predominantly present ZnO surface. This process resulted in the creation of an oxygen-deficient oxide, ultimately causing surface blackening.

Keywords: ZnO; ZnO_{1-x}; Oxidation; Oxygen-deficient oxide; Optical bandgap energy

1. Introduction

In contemporary industries, particularly in automotive, architecture, and electronics, there has been a growing demand for premium and distinctive designs featuring unique colors [1]. The significance of product color has consequently gained prominence, with consumer preferences for black products contributing to a luxurious, urban, and modern image across all age groups, resulting in a rising trend in demand [2]. Black products not only exert positive effects in terms of external aesthetics but also exhibit desirable functional characteristics, including superior heat absorption properties [3]. The prevalent method for achieving a black appearance involves the application of black coating, where the surface is painted with black pigments. This approach is widely adopted due to its ability to entirely cover the typically shiny and silver appearance of steel surfaces, often resulting from zinc (Zn) plating or zinc-alloy plating with magnesium (Mg) and aluminum (Al) [4,5]. However, challenges arise in terms of cost, necessitating thicker coatings to fully conceal the silver-white appearance. Additionally, difficulties arise in executing additional forming processes such as welding, and environmental concerns emerge due to the substantial use of coating materials, including the emission of volatile organic compounds (VOCs) [6]. Moreover, blackening through coating presents limitations in achieving performance improvements beyond the enhancement of appearance. Damages to the coating, leading to the exposure of the base material, not only compromise external aesthetics but also give rise to corrosion resistance issues [7,8]. To address these challenges, recent research has explored environmentally friendly approaches such as water vapor treatment and anodizing to achieve steel surface blackening, as opposed to traditional coating methods applied to Zn-Mg-Al alloy-plated steel sheets [4,5,9,10]. The primary focus of investigation

The Zn-Mg-Al test specimen was produced using a hot dipping method, and the nominal composition of the alloy coating is 94.5 wt.% Zn–3.0 wt.% Mg–2.5 wt.% Al. Prior to water vapor treatment, impurities on the surface were removed by degreasing using sodium hydroxide (NaOH) and ultrasonic cleaning in ethanol (C₂H₅OH). The specimen was then washed with ultrapure water with a resistance value of 18.2 MΩcm and dried completely in air. To form a black coating layer, the prepared coating was subjected to water vapor treatment for 1 hour and 30 minutes in a saturated steam atmosphere at 150°C, according to the process shown in Figure 1. The appearance of the resulting black test specimen is shown in Figure 2. and in this paper, the specimen before water vapor treatment is referred to as bare, and the specimen after water vapor treatment is referred to as black st. To elucidate the mechanism of black coating formation, the surface and cross-sectional morphology of the specimens before and after water vapor treatment were observed using FE-SEM and TEM. GD-OES and EDS was used for elemental composition analysis. The phase and crystal structure analysis were conducted using HR-XRD and XPS, and UV-VIS/NIR was used for optical property analysis, including absorbance and bandgap.





Bare	Bare ST
	
$L^* = 56.08$	$L^* = 25.22$

Figure 2. Surface observation images and whiteness of Zn-Mg-Al alloy-coated steel specimens by 150 °C water vapor treatment.

3. Results

3.1. Material Characterization

Figure 3 depicts the surface morphology of test specimens both before and after water vapor treatment. Consistent with previous findings for Zn-Mg-Al, lamellar structures are evident in the Zn-matrix phase, Zn-MgZn₂ binary, and Zn-MgZn₂-Al ternary phases, as indicated by the elements presented in the surface composition of the bare specimen in Table 1. Specifically, examination of the bare specimen's surface in Figure 3(a) reveals the presence of the Zn-matrix phase and Zn-MgZn₂-Al ternary phase [12]. Following water vapor treatment, Figure 3(b) illustrates the destruction of the lamellar structure, replaced by a diffusion-like shape. Region (3), distinguished by the highest O content and a rough surface, is presumed to have undergone the most substantial oxide formation during water vapor treatment. This suggests that the occurrence of light scattering due to surface roughness may contribute to blackening. Conversely, regions (1) and (2), retaining the lamellar structure and undergoing diffusion, exhibit comparatively less oxide formation, as indicated by the elements present in the surface composition of the Bare ST specimen in Table 2. Analysis of the oxygen composition in Bare ST suggests that an increase in the ratio of oxygen elements is associated with the advancement of blackening.

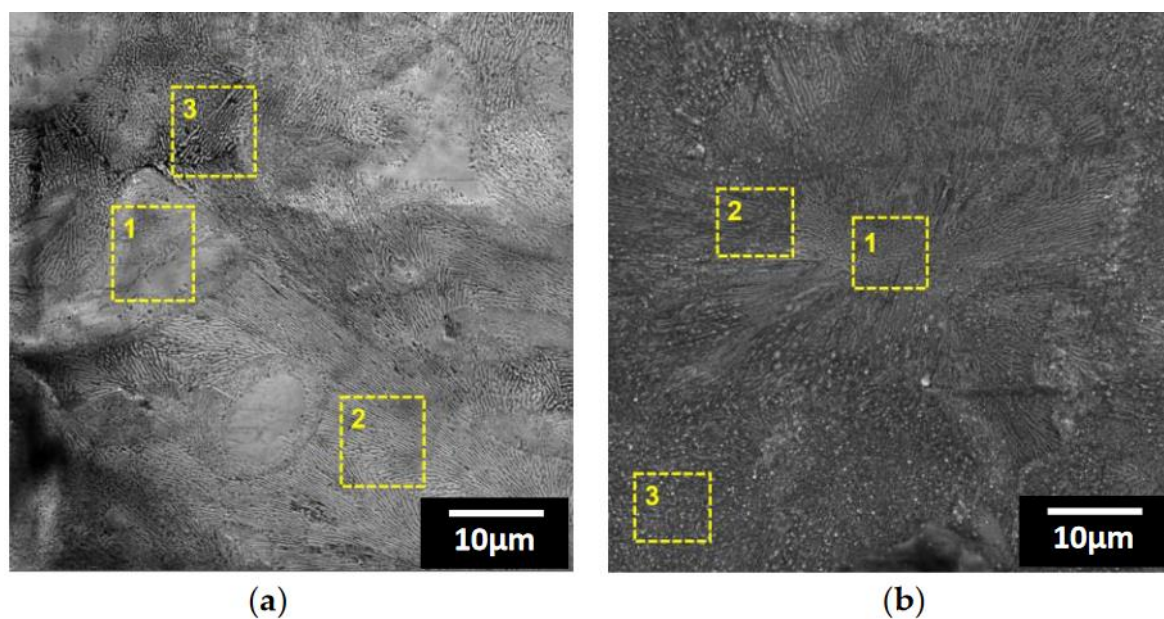


Figure 3. SEM images of surface of Bare and Bare ST; (a) Bare, (b) Bare ST.

Table 1. EDS quantitative analysis at each point marked on Figure 3. (a).

Point	Zn(at.%)	Mg(at.%)	Al(at.%)	O(at.%)
1	85.15	4.30	6.76	3.79
2	76.12	8.99	12.65	2.24
3	63.79	10.12	12.10	13.99

Table 2. EDS quantitative analysis at each point marked on Figure 3. (b).

Point	Zn(at.%)	Mg(at.%)	Al(at.%)	O(at.%)
1	43.10	9.55	12.38	34.97
2	36.94	10.28	13.75	39.03
3	30.25	8.46	16.26	45.03

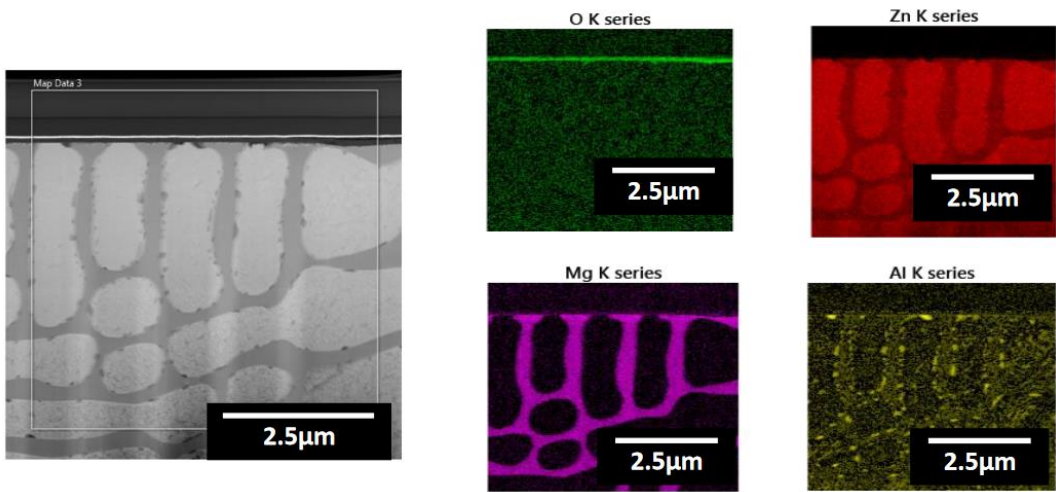


Figure 4. SEM and EDS results of Bare’s cross section.

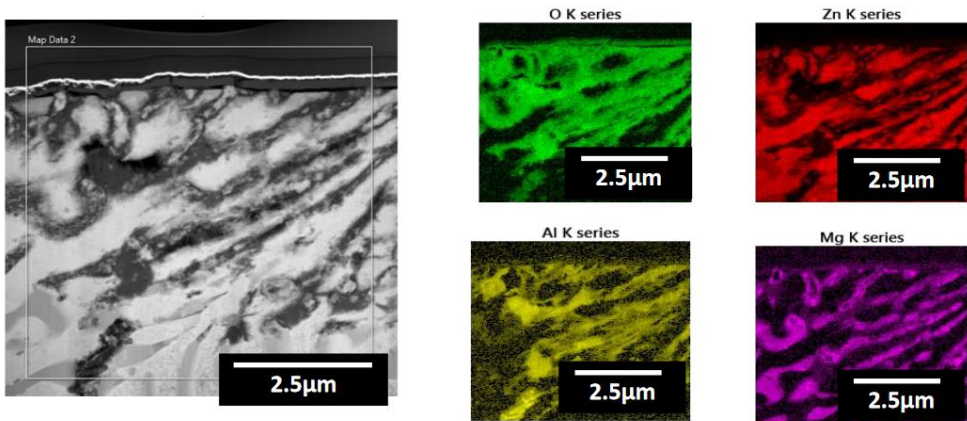


Figure 5. SEM and EDS results of Bare ST’s cross section.

Similarly to the surface morphology results observed in Figure 3, when examining the cross-sectional morphology of the Bare specimen in Figure 4, it was confirmed that a lamellar structure is formed between the intermetallic compounds. Additional TEM analysis with EDS mapping revealed predominantly formed Zn, and when confirming the point element composition in the region where Mg elements were mapped, it was determined to be 23.99 at% Mg and 71.75% Zn. This suggests the formation of the intermetallic compound $MgZn_2$. Furthermore, Al was found to be distributed around Zn and Mg, similar to the results observed on the surface. Oxygen, as seen in the mapping, was found to be extremely thin near the surface, indicating the presence of a naturally formed oxide layer on the metal surface.

In contrast, Figure 5 shows the examination of cross-sectional morphology and EDS mapping of Bare ST, where it was observed that the lamellar structure, akin to the surface morphology, was disrupted and appeared to be diffusing. This phenomenon was attributed to surface treatment occurring due to high-temperature steam. Through EDS mapping to confirm the shapes of each element, it was evident that the boundaries were clearly defined in Bare, while in Bare ST, all elements were diffused. Particularly, oxygen (O) was found to be formed approximately 5 μm deep from the surface. This led to the conclusion that an oxide layer formed through steam treatment on the surface.

Figure 6 presents the depth-wise elemental composition analysis results from the surface analyzed through GD-OES. When examining the depth-wise elemental composition of Bare, it was observed that Zn predominantly occupied the surface, consistent with the composition of the test specimen. Small amounts of Mg and Al were also detected, and Fe showed an increase from a depth of 10 μm , intersecting with the decreasing Zn, indicating the formation of an approximately 10 μm alloy coating on the specimen.

Unlike Bare, in the case of Bare ST, a higher proportion of O was observed on the surface, with the proportion gradually decreasing to a depth of about 5 μm . Additionally, the depth of the coating layer was approximately 14 μm , with a surface oxide layer of 5 μm thickness. This observation indicates an increase in the thickness of the oxide layer. This observation aligns with the results obtained through TEM's oxygen mapping, supporting the hypothesis that the main factor contributing to blackening is the formation of an oxide layer on the surface.

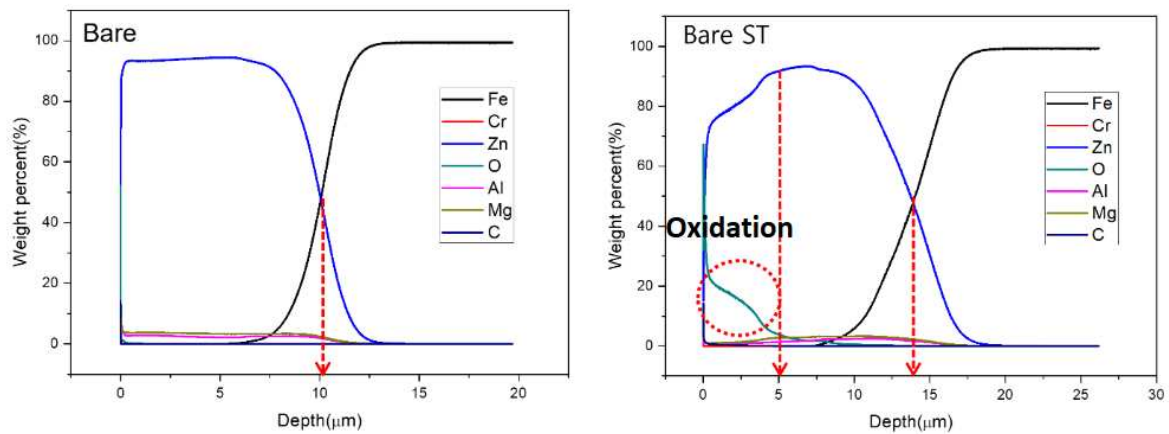


Figure 6. GD-OES depth profile for Bare and Bare ST.

Next, we analyzed the crystal structure and phase information of the test specimen film using XRD. As seen in Figure 7, peaks for mostly Zn and MgZn_2 are detected in the Bare specimen. In contrast, after the water vapor treatment, Bare ST specimen's peaks for oxides such as zinc oxide (ZnO) and hydrated oxides such as $\text{Mg}(\text{OH})_2$ were detected. It was judged that oxides were formed on the surface, similar to the EDS composition analysis, and it was confirmed that hydrated oxides were also formed on the surface. Based on the ZnO peak from the XRD analysis, the crystal size and interplanar spacing were analyzed using Bragg's law in equations 1 and 2. It was found that the interplanar spacing of ZnO increased after the water vapor treatment through Figure 8 [13]. This is presumed to result from a chemical state change or oxygen vacancy, as illustrated in Figure 9 [14].

$$L = \frac{0.9\lambda}{FWHM \cdot \cos\theta} \quad (L : \text{lattice interplanar spacing of the crystal}, \lambda : \text{wavelength of the characteristic x-ray}, \theta : \text{x-ray incidence angle}) \quad (1)$$

$$D = \frac{n \cdot \lambda}{\sin\theta} \quad (D : \text{spacing of the crystal layers}, n = \text{integer}, \lambda : \text{wavelength of the x-ray}, \theta : \text{the angle between incident ray and the scatter plane}) \quad (2)$$

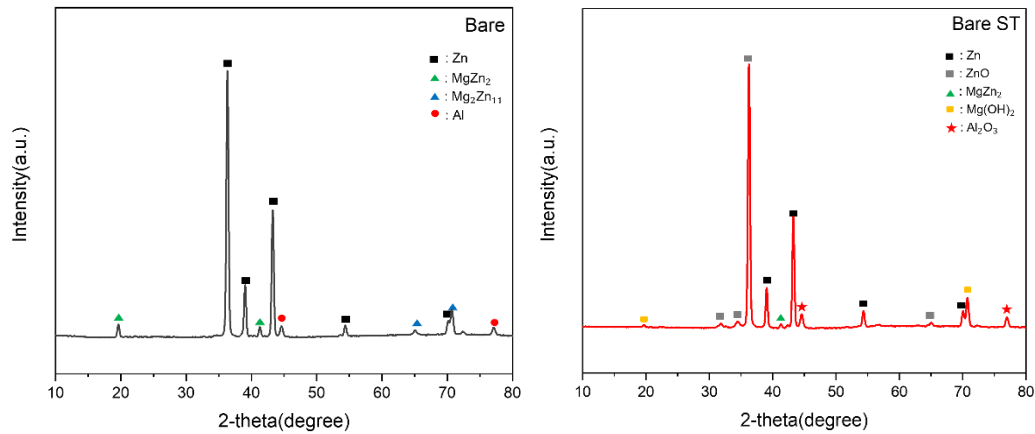


Figure 7. XRD results of Bare and Bare ST.

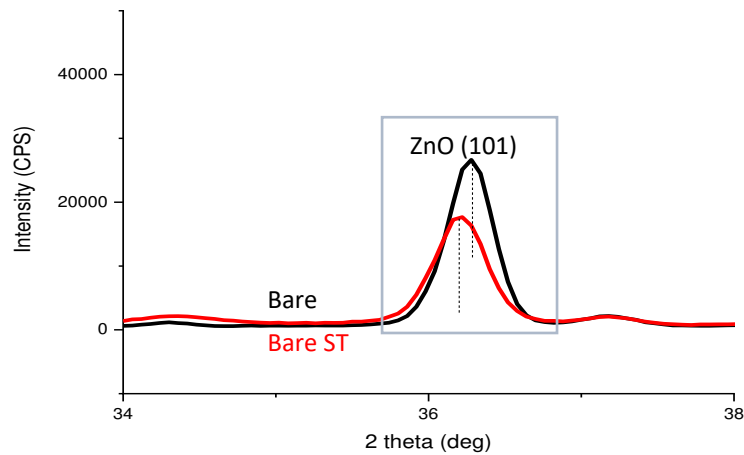


Figure 8. ZnO Lattice spacing comparison of Bare and Bare ST.

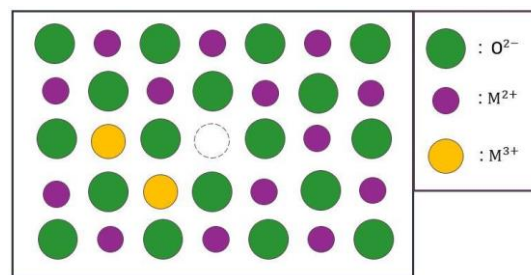


Figure 9. Schematic diagram of metal-deficient oxide with oxygen vacancy.

In addition, the crystal structure was verified through XPS spectra analysis, as illustrated in Figure 10 and Figure 11. Following water vapor treatment, discernible peaks emerged in the binding energy of the oxide and hydroxide in the Zn 2p, Mg 1s, and Al 2p results, corroborating the formation of oxide and hydroxide, in line with the findings from XRD.

Upon scrutinizing the Zn LMM spectra for the oxygen Auger peak in the Bare specimen, a peak indicative of Zn^{2+} ion binding was observed. Conversely, in the Bare ST specimen post-steam treatment, a peak corresponding to Zn^{1+} binding was identified. This observation suggests a shift in the ZnO peak after steam treatment, signifying a transformation from ZnO to ZnO_{1-x} . The alteration is likely attributed to the change in oxidation state during the transformation from ZnO to ZnO_{1-x} . Furthermore, as depicted in Figure 11, the O1s binding energy peak was subjected to fitting, revealing

three distinct peaks with binding energies of approximately 530.2, 530, and 528 eV, respectively. The lowest binding energy is associated with the metal-oxygen bond (M-O), such as ZnO or MgO, the intermediate energy corresponds to oxygen vacancy, and the highest energy is linked to the bond with moisture on the metal surface (OH) [15]. Notably, oxygen vacancy was not detected in the sample before water vapor treatment, but its occurrence was confirmed after treatment. Consequently, the observed increase in the interplanar distance of ZnO, as evidenced in the XRD results, is attributed to the occurrence of oxygen vacancy in ZnO, leading to the formation of an oxygen-deficient oxide

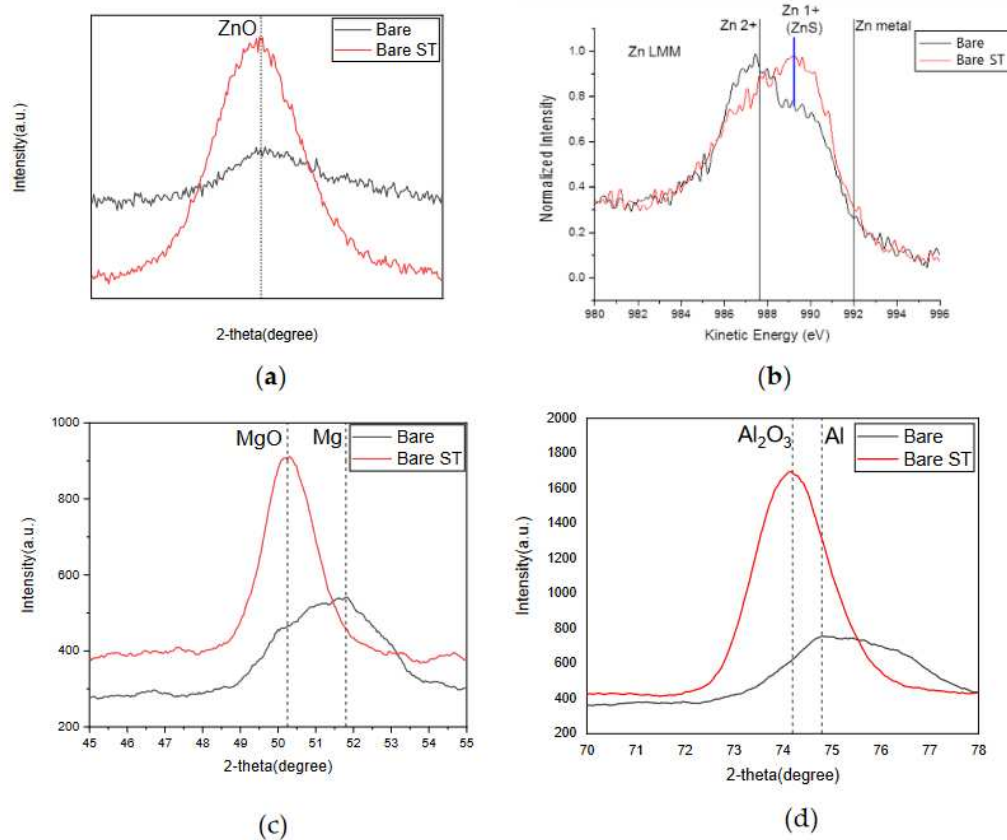


Figure 10. XPS spectra of Bare and Bare ST; (a) Zn 2p, (b) Zn LMM, (c) Mg 1s, (d) Al 2p.

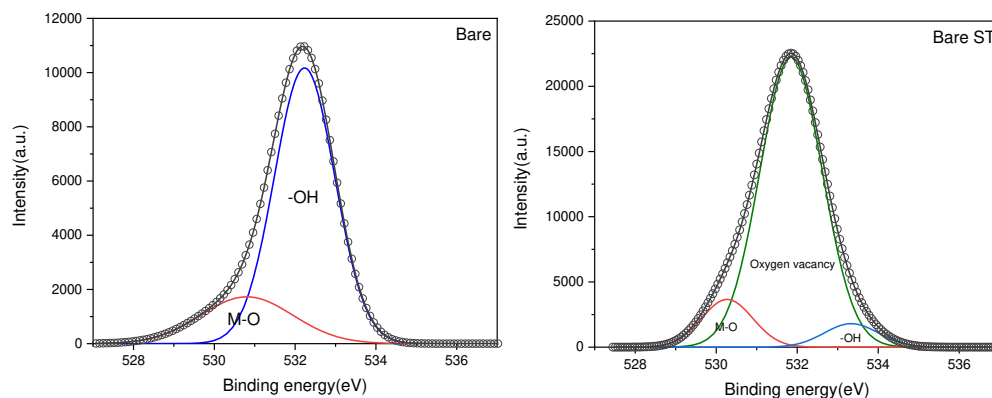


Figure 11. Bare and Bare ST's XPS spectra of O1s fitting.

(2) Optical Characterization

Figure 12 illustrates the analysis of optical properties using UV-Vis-nir to measure reflectance across the wavelength range of 0-2500 nm. Upon measuring reflectance, it was observed that the black specimen exhibited low reflectance, akin to the brightness depicted in Figure 2. For the conversion of

reflectance to absorbance, representing the extent of light absorption, the Kubelka-Munk equation (equation 3) was applied [16]. Upon examining the absorbance results, a sharp increase was observed around 390 nm in the visible light range for the black specimen after water vapor treatment, suggesting absorption of visible light by a certain factor, as depicted in Figure 12.

$$F(R) = \frac{(1-R)^2}{2R} = \frac{\alpha}{s} \quad (F(R) : \text{absorbance}, R : \text{diffuse reflectance}, \alpha : \text{absorption coefficient}, s : \text{scattering coefficient}) \quad (3)$$

This is attributed to the absorption of visible light resulting from ZnO defects caused by an increase in interfacial distance due to oxygen vacancies, as revealed in the preceding XRD and XPS analyses. In addition, the band gap was measured based on the obtained absorbance using the Tauc plot. The Tauc plot graph can be obtained by using photon energy and optical energy as the x and y axes, respectively, and the formulas for obtaining photon energy and optical energy are shown in Equation 4 and Equation 5 [17].

$$E = \frac{hc}{\lambda} \quad (E : \text{photon energy}, h : \text{Planck constant}, c : \text{speed of light}, \lambda : \text{wavelength of light}) \quad (4)$$

$$(ah\nu)^2 = 2.303 \cdot F(R) \cdot E \quad (F(R) : \text{absorbance}, E : \text{photon energy}) \quad (5)$$

Derived from the absorbance, the band gap of Bare ST was calculated to be approximately 2.92 eV, as illustrated in Figure 13. This value is lower than the typical band gap of ZnO, which is 3.4 eV, indicating that the band gap energy decreases with the proportion of oxygen in ZnO [18]. Hence, the band gap measurement implies the presence of oxygen deficiency in ZnO. As observed in Figure 14., the reactive Mg and Al ions combine with oxygen to form ZnO_{1-x} , an oxygen-deficient oxide, by extracting oxygen from ZnO.

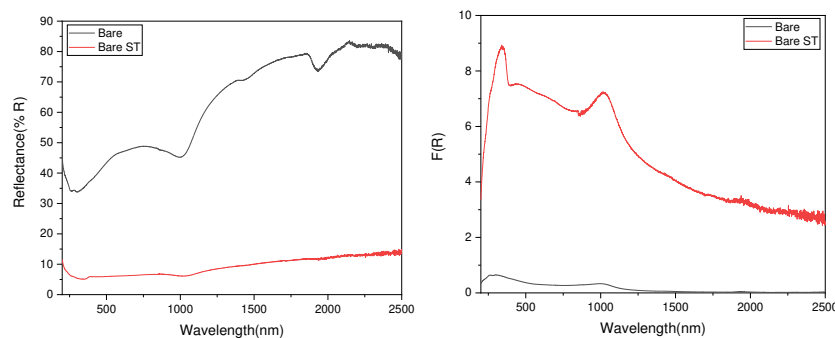


Figure 12. Reflectance and Absorbance of Bare and Bare ST.

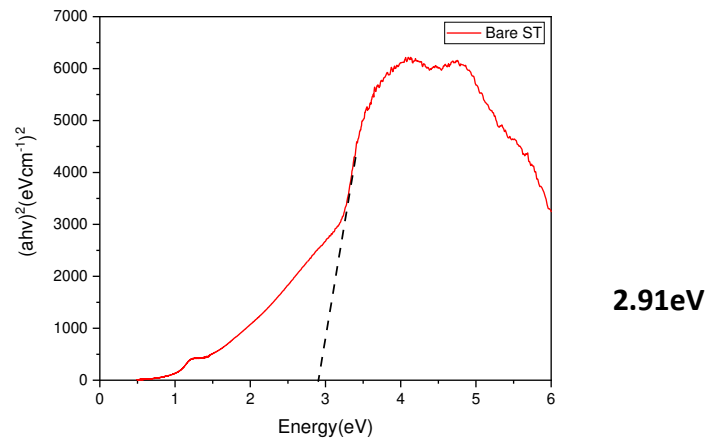


Figure 13. Band gap energy of Bare ST.

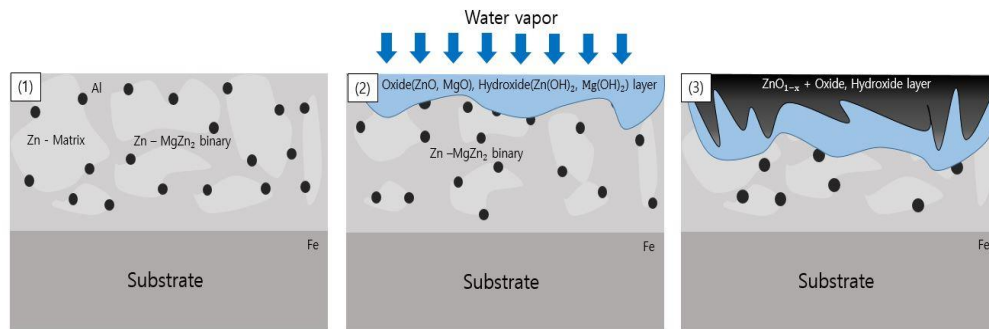


Figure 14. Schematic diagram of Zn-Mg-Al specimen's blackening.

4. Conclusions

This study delves into the mechanism of blackening on the surface of Zn-Mg-Al alloy-coated steel sheets resulting from high-temperature water vapor treatment, produced through the hot-dip galvanizing method. The findings can be succinctly summarized as follows:

- 1) Following water vapor treatment of the Zn-Mg-Al alloy-plated steel sheet, surface roughness increased, and particle size slightly grew. Examination of the surface and cross-section after water vapor treatment revealed the formation of an oxide layer, suggesting that the primary contributor to blackening is likely the influence of oxides, such as ZnO and Mg(OH)₂ in the surface layer.
- 2) Oxides and hydrated oxides were confirmed to form after water vapor treatment, leading to the creation of oxygen vacancies. This resulted in an increase in the lattice spacing of ZnO and the formation of oxygen-deficient oxide.
- 3) Measurement of the optical bandgap of the blackened test specimen yielded a value of approximately 2.9 eV, significantly lower than the 3.4 eV of ZnO. This indicates the formation of a non-stoichiometric structure, ZnO_{1-x}, due to the presence of defects. Visible light absorption by these defects is determined to be the cause of blackening.
- 4) The test specimen in this study had a composition of Zn 94.5 wt.%, Mg 3.0 wt.%, Al 2.5 wt.%. Future research should explore blackening under improved conditions by varying the ratios of Mg and Al, investigating factors promoting blackening at lower energy levels.

Author Contributions: Formal analysis, S.-H.K.; writing—original draft preparation, S.-H.K., Y.-J.K., K.-H.L., J. K., M.-H.L. and Y.-S.Y.; writing—review and editing, supervision, Y.-S.Y.; funding acquisition, Y.-S.Y. All authors have read and agreed to the published version of the manuscript.

Funding: This work was supported by the Korea Evaluation Institute of Industrial Technology(KEIT) grant, funded by the Korea Government (MOTIE), grant number 1415175139.

Institutional Review Board Statement: Not applicable.

Informed Consent Statement: Not applicable.

Data Availability Statement: Data are contained within the article.

Acknowledgments: This research was a part of the project titled 'Development of Surface Blackening Technology for High Corrosion Resistance Galvanized Alloy Coating', funded by the Ministry of Trade, Industry and Energy, South Korea.

Conflicts of Interest: The authors declare no conflict of interest.

References

1. Babolhavaej, M.; Vakilian, M.A.; Slambolchi, A. The role of product color in consumer behavior. *Advanced social humanities and management* 2015, 2, 9-15.
2. Labrecque, L.I.; Patrick, V.M.; Milne, G.R. The marketers' prismatic palette: A review of color research and future directions. *Psychology & Marketing* 2013, 30, 187-202.

3. Lee, J.; Kim, D.; Choi, C.; Chung, W. Nanoporous anodic alumina oxide layer and its sealing for the enhancement of radiative heat dissipation of aluminum alloy. *Nano energy* 2017, 31, 504-513.
4. Nakano, T.; Yamamoto, M.; Taketsu, H. 2017. Method for producing black-plated steel sheet, and method for producing molded article of black-plated steel sheet. U.S. Patent 9,598,759, March 21
5. Nakano, T.; Ueno, S.; Yamamoto, M. 2020. Method for manufacturing black plated steel sheet, apparatus for manufacturing black plated steel sheet, and system for manufacturing black plated steel sheet. U.S. Patent 10,697,053, June 30.
6. Porwal, T. Paint pollution harmful effects on environment. *Social Issues and Environmental Problems* 2015, 3, 2394-3629.
7. Nakano, T.; Yamamoto, M.; Taketsu, H. 2018. Black-plated steel sheet. U.S. Patent. 9,863,027, January 9.
8. Lee, K.H.; Jeong, J.I.; Kim, H.J.; Yang, J.H. 2023. Black plated steel sheet and manufacturing method thereof. U.S. Patent. 11,555,240, January 17
9. Kim, S.J.; Kwak, Y.J.; Kim, T.Y.; Jung, W.S.; Kim, K.Y. Surface darkening phenomenon of Zn-Mg alloy coated steel exposed to aqueous environment at high temperature. *J Mater Res* 2015, 30, 3605-3615.
10. Masuda, R.; Kowalski, D.; Kitano, S.; Aoki, Y.; Nozawa, T.; Habazaki, H. Characterization of dark-colored nanoporous anodic films on zinc. *Coatings* 2020, 10, 1014.
11. Pistofidis, N.; Vourlias, G.; Konidaris, S.; Pavlidou, E.; Stergioudis, G. The combined effect of nickel and bismuth on the structure of hot-dip zinc coatings. *Mater Lett* 2007, 61.
12. Dutta, M.; Halder, A.K.; Singh, S.B. Morphology and properties of hot dip Zn-Mg and Zn-Mg-Al alloy coatings on steel sheet. *Surface and Coatings Technology* 2010, 205, 2578-2584
13. Epp, J. X-ray diffraction (XRD) techniques for materials characterization. In *Materials characterization using nondestructive evaluation (NDE) methods* Elsevier: 2016; pp. 81-124.
14. Li, X.; Wang, Y.; Liu, W.; Jiang, G.; Zhu, C. Study of oxygen vacancies' influence on the lattice parameter in ZnO thin film. *Mater Lett* 2012, 85, 25-28.
15. Cho, S.W.; Kim, K.S.; Jung, S.H.; Cho, H.K. Towards environmentally stable solution-processed oxide thin-film transistors: a rare-metal-free oxide-based semiconductor/insulator heterostructure and chemically stable multi-stacking. *Journal of Materials Chemistry C* 2017, 5, 10498-10508.
16. Shen, J.; Li, Y.; He, J. On the Kubelka-Munk absorption coefficient. *Dyes and Pigments* 2016, 127, 187-188.
17. Jubu, P.R.; Obaseki, O.S.; Nathan-Abutu, A.; Yam, F.K.; Yusof, Y.; Ochang, M.B. Dispensability of the conventional Tauc's plot for accurate bandgap determination from UV-vis optical diffuse reflectance data. *Results in Optics* 2022, 9, 100273.
18. Dostanko, A.P.; Ageev, O.A.; Golosov, D.A.; Zavadski, S.M.; Zamburg, E.G.; Vakulov, D.E.; Vakulov, Z.E. Electrical and optical properties of zinc-oxide films deposited by the ion-beam sputtering of an oxide target. *Semiconductors* 2014, 48, 1242-1247.